PROCEEDINGS OF SCIENCE

Fermi-LAT Observation of 3C 454.3 during its 2014 May-July outburst

Richard J. Britto*
Department of Physics, University of Johannesburg, Auckland Park 2006, South Africa
E-mail: rbritto@uj.ac.za

Sara Buson
Istituto Nazionale di Fisica Nucleare, Sezione di Padova, I-34131, Padova, Italy
Dipartimento di Fisica "G. Galilei", Università di Padova, I-34131, Padova, Italy
Current affiliations:
Astrophysics Science Division, NASA Goddard Space Flight Center, Greenbelt, MD 20771 USA
University of Maryland Baltimore County/CRESST, Baltimore, MD 21250, USA
E-mail: sara.buson@nasa.gov

Benoît Lott
Univ. Bordeaux, Centre d'Études Nucléaires de Bordeaux-Gradignan, UMR 5797,
CNRS/IN2P3, 33175 Gradignan, France, lott@cenbg.in2p3.fr
E-mail: lott@cenbg.in2p3.fr

Soebur Razzaque
Department of Physics, University of Johannesburg, Auckland Park 2006, South Africa
E-mail: srazzaque@uj.ac.za

Eugenio Bottacini
W. W. Hansen Experimental Physics Laboratory, Stanford University, Stanford, CA 94305, USA

Flat Spectrum Radio Quasar 3C 454.3 is the brightest active galactic nucleus to have been detected in the γ-ray spectral band. It was observed in an outburst phase during 2014 May-July, and a large amount of data was collected with the *Fermi*-Large Area Telescope (*Fermi*-LAT) from 100 MeV to several tens of GeV. In its nominal sky-survey operating mode, *Fermi*-LAT can see the whole sky every 3 hours, which allowed us to draw detailed light curves during its flaring period, and perform spectral analysis during some specific sub-flares. During these periods, we observed the following features: a fast variability; a hard spectral index close to $\Gamma = 2.0$, by fitting spectral energy distributions with a single power law model > 100 MeV; the highest flux at a level of F[E>100 MeV] = $21.6 \pm 2.6 \times 10^{-6}$ photons cm^{-2} s^{-1}; several photons at high energies beyond 20 GeV. We will present upper limits on the estimation of the Doppler factor δ and discuss constraints on the location of the γ-ray emitting region.

3rd Annual Conference on High Energy Astrophysics in Southern Africa -HEASA2015,
18-20 June 2015
University of Johannesburg, Auckland Park, South Africa

*Speaker.

PoS(HEASA2015)021

1. Introduction

Flat spectrum radio quasar (FSRQ) 3C 454.3 is one of the brightest active galactic nuclei (AGNs) in the γ-ray energy band. It is abundantly studied for several years in all wavelengths, and particularly in the MeV and GeV domain since the launch of the AGILE and Fermi γ-ray space telecopes, in 2007 and 2008 respectively [23, 24, 1]. An interesting review on blazar modeling was presented by Finke [13].

FSRQ 3C 454.3 is modeled, in the context of the unified model of AGNs, as a supermassive black hole surrounded by an accretion disk at the centre of a host galaxy, and its brightness outshines the brightness of the stars of its host galaxy. It also exhibits a pair of narrow jets that are believed to be due to the presence of a strong magnetic field surrounding the supermassive black hole. 3C 454.3 is a blazar, i.e., a radio quasar having one of its relativistic plasma jets directed close to the Earth direction, that makes this object extremely bright, particularly during periods of elevated activity.

Blazar 3C 454.3 was intensively monitored for several years, and many studies reported several characteristic stuctures: a three-phase outburst flux level, a flaring behaviour showing rapid variability while reaching several times the flux of the source in its quiescent state, a spectral break in the spectral energy distribution (SED) around 1-2 GeV, high energy photons towards the end of the flaring episode, and various constraints on the location of the γ-ray emiting region (e.g. [2, 5, 3, 11, 17, 16]). A more detailed (but not exhaustive) review on previous results on 3C 454.3 is given in Britto et al. [8].

A flat Λ-CDM cosmology with $H_0 = 69.6$ km s^{-1} Mpc^{-1}, $\Omega_m = 0.286$, and $\Omega_\Lambda = 0.714$ is used in this paper [18].

2. Observations and analysis

The *Fermi* Large Area Telescope (*Fermi*-LAT) is a pair-conversion space telescope sensitive to γ-ray photons from $\sim$20 MeV to $\sim$300 GeV. It was launched on 2008 June 11, and has supplied a considerable amount of data from a variety of high energy sources [4], among them 1563 AGNs at high Galactic latitudes, as reported in the 3LAC [6]. For most of its observation time, the spacecraft operates in a survey scanning mode, enabling the LAT to see the whole sky every 3 hours, corresponding to two orbits of the instrument.

The 2014 May-July outburst was studied from May 20 to July 25 (MJD 56815.0-56863.0), along with a preceeding period of quiescent activity (called "pre-flare"), ranging from 2013 Oct 5 to 2014 May 20 (MJD 56570.0-56797.0, Table 1). LAT data from these periods were analysed using the Fermi Science Tools version v9r33p0, publicly available[1], and the Pass 7 REPROCESSED data representation. Signal from 3C 454.3 was reconstructed using the unbinned likelihood algorithm of the gtlike/pyLikelihood software package, and the P7REP_SOURCE_V15 set of instrument response functions. Only photons with energies greater than 100 MeV were considered in this analysis. An event selection with zenith angle $\theta_z \leq 100^\circ$ was applied in order to avoid contamination from γ rays coming from the Earth limb.

[1] http://fermi.gsfc.nasa.gov/ssc/data/analysis/software/

Table 1: Outburst phases of 3C 454.3, as identified from the light-curves.

	Phase	Dates	MJD	Duration (days)
1	Pre-flare	2013 Oct 5 - 2014 May 20	56570.0 - 56797.0	227.0
2	Plateau	2014 May 20 - 2014 Jun 7	56797.0 - 56815.0	18.0
3	Flare	2014 Jun 7 - 2014 Jun 29	56815.0 - 56837.0	22.0
4	Post-flare	2014 Jun 29 - 2014 Jul 25	56837.0 - 56863.0	26.0
3a	Flare I	2014 Jun 10 - 18 Jun	56818.5 - 56826.5	8.0
3b	Flare II	2014 Jun 20 - 25 Jun	56828.0 - 56833.5	5.5

In the analysis presented in this paper, photons were selected in a 10° circular region of interest (ROI), centered at the position of 3C 454.3. The isotropic background, including the sum of residual instrumental background and extragalactic diffuse γ-ray background, was modeled by fitting this component at high Galactic latitude (file "iso_source_v05.txt" provided with the *Fermi Science Tools*). The "gll_iem_v05_rev1" Galactic diffuse emission model was used. All point sources in the third *Fermi*-LAT source catalog (3FGL, [4]) located in the ROI and an additional surrounding 10° wide annulus (called "source region") were modeled in the fits, with the spectral parameters kept free only for the brightest sources in the ROI. Depending on the type (spectral or time domain) of analysis, either two or four point sources fit the criteria for "brightest sources", corresponding to a detection significance of TS>20 in the 3FGL. Light-curves were produced by using a single power law spectral (PL) model of our source of interest, though curvatures and breaks are known to be characteristic of the spectral shape of 3C 454.3 in the *Fermi*-LAT energy band. The use of this simpler model allows us to analyse low statistic (sparse) data set with smaller uncertainties. Spectral studies were performed by using the following spectral shapes: *broken power law (BPL)*, *log-parabola (LP)* and *power law with an exponential cutoff (PLEC)*, as defined in [8].

Five data sets from the *Swift*-XRT X-ray space telescope were collected at MJD 56822.27, 56824.60, 56825.67, 56826.13 and 56829.60, whose durations between 26 and 66 min during five different epochs of the main γ-ray flare. However, due to large uncertainties in the flux calculations, we only used an average X-ray flux during the flare episode, obtained by fitting the light-curve of the five values of the flux, which remains almost constant. From a fit by a constant function, we obtained the value $F[2-6\,\mathrm{keV}] = (2.06 \pm 0.95) \times 10^{-11}$ erg cm^{-2} s^{-1}, in the 2–6 keV range. More details on the X-ray data extraction were given in [8].

3. Time-domain analysis

Due to the high flux of 3C 454.3 we observed during the June 7–29 period, we studied light-curves in a 3-hr binning, unveilling a multiple peak structure, and showing a dramatically fast variability pattern, for which six major peaks were labeled on Figure 1. A harder spectral index associated with the detection of high energy photons during the flare and post-flare phases seems to be a common feature of high-state activity for 3C 454.3. We observed that the highest flux is reached during MJD 56823 (maximum of Peak 3), with the value $F_{100} = 21.6 \pm 2.6$ (with F_{100} in units of 10^{-6} photons cm^{-2} s^{-1}), associated with PL index $\Gamma = 2.1 \pm 0.1$, at 56823.5625. Hard spectra with $\Gamma < 2$ are observed at the end of Peak 4, 5 and 6. The lowest values of the photon index

$\Gamma = 1.8 \pm 0.1$ are observed at MJD 56832.0625, 56827.6875, 56832.9375, 56834.0625, 56836.4375 and 56836.6875.

In order to quantify the fast variability of the signal, we fitted this detailed structure by modeling each of the peaks with a flux $F_{100} > 6$ by a two component exponential function F, such that:

$$F = 2F_0(e^{(t_0-t)/T_r} + e^{(t-t_0)/T_f})^{-1}, \tag{3.1}$$

where:

- t_0 is the time of the peak value;
- T_r and T_f are the rise and fall time, respectively;
- F_0 is the flux at t_0, representing the subflare amplitude

A constant component to model the baseline is also added to the sum of the modeled peak functions. We studied the six prominent peaks and reported their fitting parameters in Table 2. From our best fit model, we obtained a rise time $T_r = 0.04 \pm 0.02$ day ($\sim$ 1 hr $\pm$ 30 min), associated with Peak 4, centered at t_0=56827.125, though the large statistical error associated with this parameter allows significantly different values. Peaks 2 and 5 are the broadest peaks, both reaching $F_{100} \simeq 16 \pm 2$ with their T_r and T_f of the order of one day.

Since these results indicate rising times well below the LAT survey period of 3 hr, the bin size we used on Figure 1 only shows an average flux over a time period for which the exposure pattern of the source of interest is significantly variable. To remove the systematic effect caused by the exposure change, we extended the unbinned likelihood algorithm to the time domain, by fitting a time-dependent function to the data that are now not binned in energy, or in time. The time function is of the form $S_S(E,t) = S(E) \times (F(t) + B)$, where $F(t)$ is given in Eq. 3.1, B is a continuous component and $S(E)$ is a power-law distribution (with fixed photon index, hence neglecting the spectral changes during the flare). To compute the likelihood, the needed instantaneous exposure rate was interpolated from the values assessed every 30 s (same time steps as in the spacecraft data file provided by the *Fermi Science Support Center*). This method was applied to study the fast variability of Peak 1 and 4, as shown on Figure 3. Peak 1 is shown on the left panel. On the top panel is the LAT exposure on 3C 454.3, and on the botton panel the 3-hr and 6-hr light-curves, along with the function fit of the 3-hr light-curve (black) and unbinned data (red). To be able to verify the fit quality, on the middle panel is given the comparison between the counts of photons ascribed to the source between the data (blue) and the estimate from the fitted function (red) is given in the middle panel. The unbinned method gives $T_r = 3.8 \pm 1.1$ ks (1.06 ± 0.31 hr), $T_f = 17 \pm 4$ ks (4.72 ± 1.11 hr). For the MJD 56827 flare ("Peak 4"), the unbinned method yields $T_r = 1.0 \pm 0.5$ ks (0.28 ± 0.14 hr) and $T_f = 24 \pm 4$ ks (6.67 ± 1.11 hr). T_r in Peak 4 is the shortest timescale reported for this source in the γ-ray band. These results are not always matching the results of the conventional fit we reported on Figure 1 and Table 2, since we used a method that defines uncertainties better when applied to small time scales. Unexpectedly, this flare peaks in flux almost exactly simultaneously with a change in scanning mode. The accuracy and robustness of the analysis have been checked with Monte-Carlo simulations, and we verified that Peak 4 is

not influenced by the change in scanning mode. Inspection of the data did not reveal any change in background during this flare that could have biased our results.

In the bottom panel of both Fig. 1 the high energy (HE) photons above 10 GeV are presented along with the light-curves. To identify γ-ray induced events with a high degree of accuracy, we use the "ULTRACLEAN" class of events. We report events at energies E $>$ 10 GeV, along with their arrival time and a probability $>$ 0.9545 (2-σ Gaussian equivalent) to be associated with 3C 454.3, within a ROI = 0.5°. The way HE photons are distributed during the flare phase (phase 3) is clearly visible in Fig. 1. Most of the HE photons are detected during the second part of this phase, mainly after Peak 3. No HE photons were detected during Peak 1. Moreover, the bulk of HE photons is detected in the second half of the broad structures, like in both the Peak 2-Peak 3 and Peak 5 subflares. Around the maximum of Peak 5, we found one photon at E = 34.6 GeV (MJD 56830.7616), associated with a probability 0.99999. Around the maximum of Peak 4, we found one photon at E = 43.3 GeV, associated with a probability 0.99998, which was detected at MJD 56827.1233, i.e., 4.5 ks (1.2 h) after the flux peak.

Spectral analysis was performed by producing a SED for each of the outburst episodes reported in Table 1, namely period (1, 2, 3, 3a, 3b, 4), as well as for Peaks 2, 3, 4 and 5 that constitute major subflare events. Binned SEDs were fitted by PL, BPL, LP and PLEC functions. The total integrated fluxes (F_{100}) have been computed, and are displayed in Fig. 2, showing the dependence of the photon spectral index Γ on the flux for phases 1, 2, 3a, 3b and 4, for the PL fit (left panel) and BPL fit (right panel). The "harder when brighter" spectral property we already mentioned is clearly observable through these different phases of the outburst. Results from the spectral analysis of Peaks 2, 3, 4 and 5 are reported in Table 3, where hardening of the PL spectral indices Γ are quantified as $\Gamma \simeq 1.9$ for Peak 4, and $\Gamma \sim 2$ for Peak 2, 3 and 5.

The integrated apparent luminosity L of the source was calculated for each of the three spectral shapes (BPL, LP and PLEC), and are also reported in Table 3. Since we found photons up to the 40-60 GeV energy bin in the analysis of 6 years of 3C 454.3's data [8], we chose to calculate L in the 0.1-60 GeV energy range, according to the following formula:

$$L = 4\pi d_L^2 \int_{E_1}^{E_2} E \frac{dN(E)}{dE} dE, \tag{3.2}$$

with E_1=100 MeV, E_2=60 GeV, the luminosity distance d_L = 5.55 Gpc = 1.71×10^{28} cm, using the cosmological parameters defined in Section 1, and $dN(E)/dE$ the differential form of the spectral model we have used. The highest values of the luminosity are found for Peak 3, at $L \simeq 33 \times 10^{48}$ erg s^{-1}.

4. Discussion

The 2014 May-July outburst of 3C 454.3 looks similar to previous bright flares of this source reported with Fermi-LAT in the recent years. These similarities includes: a three phase pattern, a spectral break around 1-2 GeV, fast variability and a multi-peak structure of the light-curve during the main flare. However, though the flux in 2014 was far below its level of 2010 November, we reported some characteristics that are particularly interesting and unique to this 2014 May-July flare, to the best of the authors' knowledge: a main flare that lasted for 22 days (June 7-29) with

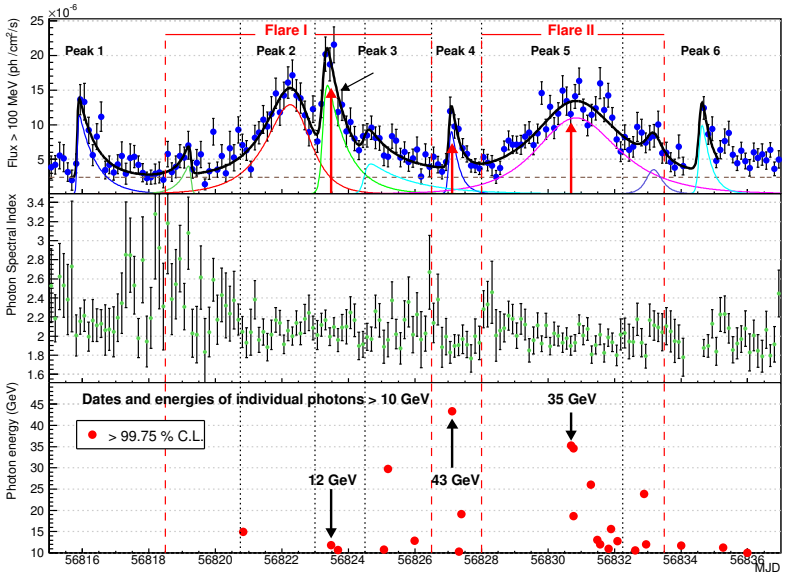

Figure 1: (Top panel) *Fermi*-LAT light-curve of the flare phase with 3-hr binning. Flaring peaks were fitted by the F function (in Eq. 3.1) for 9 structures. Fits were performed in the MJD 56815.625-56835.130 time range. The thin colored lines correspond to the contribution of single peaks to the total fit, which is represented by the black thick line. The dashed brown line is the fitted constant baseline, which also contributes to the total fit. Six major peaks were labeled for more detailed studies. The red arrows indicate the position of the three high energy photons used to calculate the Doppler factor in section 4 (Discussion), and whose energy are labeled in the bottom panel. Due to an instrumental problem, the MJD 56834.375 bin contains no data. *Middle panel:* Photon spectral index (Γ) of the PL fits of data. *Bottom panel:* Photons above 10 GeV with two different significance levels of source association (2- and 3-σ Gaussian equivalent). Vertical red dashed lines indicate the two major flaring phases (I and II), and black dotted lines Peaks 2, 3, 4 and 5.

Table 2: Parameters of fit function F, for the 6 peaks identified on figure 1. A constant baseline flux of $(2.4 \pm 0.6) \times 10^{-6}$ ph cm^{-2} s^{-1} was also fitted to the data. The χ^2/ndf for the whole fit is 1.27.

Peak	t_0 (MJD)	F_0 (10^{-6} *ph cm*$^{-2}$ *s*$^{-1}$)	T_r (hr)	T_f (hr)
1	56815.8477	6.6± 1.1	0.5± 0.1	12.6± 2.8
2	56822.3984	12.5± 0.9	18.4± 1.9	11.0± 1.8
3	56823.2422	10.5± 1.5	1.4± 0.7	15.1± 2.3
4	56827.0391	6.7± 1.3	0.9± 0.5	5.6± 1.1
5	56830.7305	10.9± 0.6	23.8± 1.9	29.2± 2.6
6	56834.5625	7.5± 0.5	1.1± 1.0	6.6± 2.1

a better defined peak structure than in November 2010, a hard power law photon index $\Gamma \sim 2$ throughout the whole main flare episode, the detection of a 43-GeV photon on MJD 56827.1233. A rise time of $\sim$1000 s (at MJD 56827) was reported for the first time during a MeV-GeV flare of 3C 454.3, which represents one of the shortest flux variability time measured for blazars in this energy range. Also, its flux reached an average value of $F_{100} = 7.2 \pm 0.2$ during 2014 June 7–29,

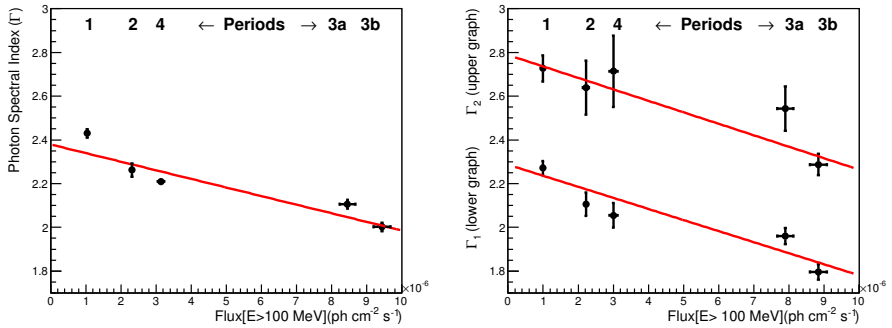

Figure 2: Photon spectral index *versus* F_{100} for five phases of the outburst: pre-flare, plateau, flare I, flare II and post-flare, as defined in Table 1. *Left panel:* Fluxes are calculated with PL model of photon index Γ. *Right panel:* Fluxes are calculated with BPL model of photon indices Γ_1 and Γ_2.

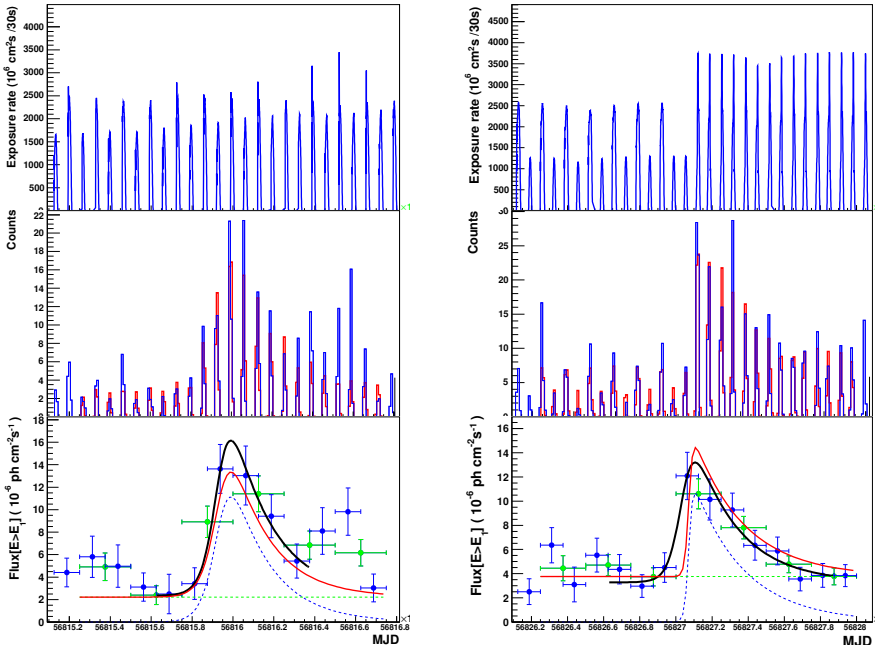

Figure 3: *Left panel:* MJD 56816 ("peak 1") flare. *Top:* Exposure rate as a function of time. *Middle:* Measured (probability-weighted, blue) and modeled (red) photon counts. *Bottom:* light-curves. Blue points: 3-hr binning, green points: 6 hr-binning. Black curve: function fitted to 3-hr points. Red curve: function fitted using the unbinned method. *Right:* Same for the MJD 56827 ("peak 4") flare.

which is similar to the 2010 April flare. The peak flux, $F_{100} = 21.6 \pm 2.6$ was recorded on 2014 June 15 (MJD 56823.5625) in a 3-hr light-curve.

The dramatic flux variations we reported in this paper could indicate that γ rays are being emitted from compact regions (called "blobs") located withing the blazar's jet. The radii of these blobs in the comoving frame, $R' \approx \delta c t_v/(1+z)$, depend on their Doppler factor δ and the time

Table 3: Parameters of the PL, BPL, LP and PLEC fit functions obtained by the likelihood analysis for Peaks 2, 3, 4 and 5. These parameters are defined in Eq. 1-4. The quality of unbinned fits is given by the $Log(likelihood)$ for each of these three fitting functions, for the PL model, along with other fit parameters. For the LP, BPL and PLEC models, values of $\Delta Log(likelihood)$ are given, with respect to $Log(likelihood)$ of the PL fit. Luminosity was estimated according to the formula of Eq. 3.2.

PL	date (MJD)	$F[>100$ MeV] (10^{-6} ph cm^{-2} s^{-1})		Γ			$-Log(likelihood)$
Peak 2	56820.75-56823.00	11.1 ± 0.5		2.06 ± 0.03			10093.1
Peak 3	56823.00-56824.50	12.4 ± 0.6		2.08 ± 0.04			7181.1
Peak 4	56826.50-56828.00	5.8 ± 0.4		1.94 ± 0.04			5858.4
Peak 5	56828.00-56832.25	9.7 ± 0.3		2.00 ± 0.02			23202.7
BPL	date (MJD)	$F[>100$ MeV] (10^{-6} ph cm^{-2} s^{-1})	Luminosity (10^{48} erg s^{-1})	Γ_1	Γ_2	E_{break}	$\Delta\, Log(likelihood)$
Peak 2	56820.75-56823.00	10.3 ± 0.5	31.0	1.85 ± 0.06	2.40 ± 0.09	1000 ± 100	-11.4
Peak 3	56823.00-56824.50	11.7 ± 0.6	33.4	1.93 ± 0.06	2.50 ± 0.14	1500 ± 100	-6.8
Peak 4	56826.50-56828.00	5.4 ± 0.4	20.1	1.78 ± 0.07	2.39 ± 0.17	1900 ± 200	-1.7
Peak 5	56828.00-56832.25	9.1 ± 0.3	31.3	1.79 ± 0.04	2.28 ± 0.05	1000 ± 100	-22.7
LP	date (MJD)	$F[>100$ MeV] (10^{-6} ph cm^{-2} s^{-1})	Luminosity (10^{48} erg s^{-1})	α	β		$\Delta\, Log(likelihood)$
Peak 2	56820.75-56823.00	10.1 ± 0.5	29.9	1.81 ± 0.06	0.12 ± 0.03		-13.8
Peak 3	56823.00-56824.50	11.6 ± 0.6	34.3	1.91 ± 0.07	0.08 ± 0.03		-5.0
Peak 4	56826.50-56828.00	5.4 ± 0.4	21.3	1.75 ± 0.09	0.08 ± 0.03		-3.9
Peak 5	56828.00-56832.25	9.0 ± 0.3	30.2	1.76 ± 0.04	0.11 ± 0.02		-28.5
PLEC	date (MJD)	$F[>100$ MeV] (10^{-6} ph cm^{-2} s^{-1})	Luminosity (10^{48} erg s^{-1})	Γ_{PLEC}	E_{cutoff}		$\Delta\, Log(likelihood)$
Peak 2	56820.75-56823.00	10.4 ± 0.5	29.2	1.84 ± 0.06	6700 ± 1800		-14.8
Peak 3	56823.00-56824.50	11.8 ± 0.6	33.1	1.93 ± 0.06	10500 ± 4200		-6.5
Peak 4	56826.50-56828.00	5.5 ± 0.4	21.0	1.81 ± 0.07	16300 ± 7900		-4.5
Peak 5	56828.00-56832.25	9.3 ± 0.3	30.0	1.83 ± 0.03	10800 ± 2200		-25.6

scale t_v over which their flux vary, *e.g.* [12]. The value of δ can be constrained by requiring the blob to be optically thin to GeV photons that may be absorbed through the $\gamma\gamma \rightarrow e^{\pm}$ pair production process. For each peak (associated to a single blob), the lower limit of delta is then obtained by computing the interaction of the highest energy photon detected in the peak, with the radiation field we modeled by fitting the X-ray to γ-ray SED we obtained for the same subflaring episode, by combining XRT and LAT data, assuming that this whole radiation field is produced in the same blob. The details of this calculation, following Gould and [14] and [9], are given in [8]. We calculated the Doppler factor δ for Peak 3, Peak 4 and Peak 5, associated to high energy photons at 12, 43 and 35 GeV respectively. To represent the flux variability time t_{var}, we use the value $T_r = 1.4$ hr for Peak 3 and $T_r = 23.8$ hr for Peak 5, obtained with the conventional fit (Table 2), and $T_r = 0.33$ hr for Peak 4, obtained from the fastest variability study. We calculate $\delta \gtrsim 20$, 31 and 14, for Peak 3, Peak 4 and Peak 5 respectively. While the δ values for Peak 3 and Peak 5 are similar to the ones obtained for the 2010 November flare, the value $\delta \gtrsim 31$ for Peak 4 can give interesting constraints. Observations from long-term Very Long Baseline Interferometry (VLBI) inferred an average value of the angle between the jet and our line-of-sight to be $\theta = 1.3^{\circ}$ [15]. Using $\delta = [\Gamma_{\rm jet}(1-\beta_{\rm jet}\cos\theta)]^{-1}$, we calculate the values of the Lorentz factor $\Gamma_{\rm jet} = 11$, 18 and 7, for Peak 3, Peak 4 and Peak 5 respectively. The value for Peak 4 is similar to the ones reported by Jorstad et al. [15] and in Sikora et al. [19]. Using $\beta_{\rm jet} = \sqrt{\Gamma_{\rm jet}^2 - 1}/\Gamma_{\rm jet}$, we can infer values of $\beta_{\rm jet}$.

Table 4: Values of δ, $\beta_{\rm jet}$, R', $\Gamma_{\rm jet}$ and r, corresponding to the Peak 3, Peak 4 and Peak 5 subflaring events.

Subflaring events	δ	$\beta_{\rm jet}$	$\Gamma_{\rm jet}$	R'	r [cm]
Peak 3	20	0.996	11	1.6×10^{15}	1.8×10^{16}
Peak 4	31	0.998	18	5.0×10^{14}	1.1×10^{16}
Peak 5	14	0.990	7	1.9×10^{16}	1.4×10^{17}

We can also calculate the distances r of the γ-ray emitting blobs from the supermassive black hole from the previously calculated Lorentz factors $\Gamma_{\rm jet}$, as $r \simeq 2\Gamma^2_{\rm jet} c t_v/(1+z)$. This would give distances $r \gtrsim 1.8 \times 10^{16}$ cm, $\gtrsim 1.1 \times 10^{16}$ cm and $\gtrsim 1.4 \times 10^{17}$ cm, for Peak 3, Peak 4 and Peak 5 respectively. The estimated values of δ, $\beta_{\rm jet}$, $\Gamma_{\rm jet}$, R' and r are reported in Table 4.

Comparing these characteristics of the three Peaks gives us an interesting picture of the flare evolution throughout June 7 to 29, by constraining physical parameters associated to the jet and blob evolutions. In the context of multiple γ-ray emitting blobs for different Peaks in the LAT light-curves, the lack of high energy photons for the first 8 days of the flare (including Peak 1 and 2) points towards blobs that are optically thick to $\gamma\gamma$ pair production, and are slower than those blobs responsible for the Peaks 3, Peak 4 and Peak 5. Peaks 3, 4 and 5 are found indeed fast and optically thin to $\gamma\gamma$ pair production, as suggested by the emission of several photons beyond 10 GeV (at these energies the pair production process is expected to happen). The distances r from the supermassive black hole we calculated would locate these blobs in the outer layers of the canonical broad-line region that surrounds FSRQs. The radius of the broad-line region was estimated to be $R_{BLR} < 10^{18}$ cm, for 3C 454.3 [7, 20].

Note: At the time of finalizing this document, we came to know about the work of Coogan, Brown and Chadwick [10], who reported similar findings.

Acknowledgments

The *Fermi*-LAT Collaboration acknowledges support for LAT development, operation and data analysis from NASA and DOE (United States), CEA/Irfu and IN2P3/CNRS (France), ASI and INFN (Italy), MEXT, KEK, and JAXA (Japan), and the K.A. Wallenberg Foundation, the Swedish Research Council and the National Space Board (Sweden). Science analysis support in the operations phase from INAF (Italy) and CNES (France) is also gratefully acknowledged. E. B. acknowledges NASA grants NNX13AO84G and NNX13AF13G. R. J. B. and S. R. acknowledge support from the National Research Foundation, South Africa and the South African Gamma-ray Astronomy Programme (SA-GAMMA).

References

[1] A. A. Abdo, M. Ackermann, M. Ajello, et al., *Early Fermi Gamma-ray Space Telescope Observations of the Quasar 3C 454.3*, *ApJ*, **699** (2009), pp. 817-823

[2] A. A. Abdo, M. Ackermann, M. Ajello, et al., *Spectral Properties of Bright Fermi-Detected Blazars in the Gamma-Ray Band*, *ApJ*, **710** (2010), pp. 1271-1285

[3] A. A. Abdo, M. Ackermann, M. Ajello, et al., *Fermi Gamma-ray Space Telescope Observations of the Gamma-ray Outburst from 3C454.3 in November 2010*, *ApJL*, **733** (2011), pp. L26-L32

[4] F. Acero, M. Ackermann, M. Ajello, et al., *Fermi Large Area Telescope Third Source Catalog*, *ApJS*, **218** (2015), pp. 23-63

[5] M. Ackermann, M. Ajello, L. Baldini, et al., *Fermi Gamma-ray Space Telescope Observations of Gamma-ray Outbursts from 3C 454.3 in 2009 December and 2010 April*, *ApJ*, **721** (2010), pp. 1383-1396

[6] M. Ackermann, M. Ajello, W. B. Atwood et al., *The Third Catalog of Active Galactic Nuclei Detected by the Fermi Large Area Telescope*, *ApJ*, **810** (2015), pp. 14-47

[7] G. Bonnoli, G. Ghisellini, L. Foschini, F. Tavecchio and G. Ghirlanda, *The γ-ray brightest days of the blazar 3C 454.3*, *MNRAS*, **410** (2011), pp. 368-380

[8] R. J. G. Britto, S. Buson, S., B. Lott, S. Razzaque, & E. Bottacini, *Fermi-LAT Observations of 2014 May-July outburst from 3C 454.3*, Submitted to *ApJ*, arXiv:1511.02280 [astro-ph.HE] (2015), 15 pages

[9] R. W. Brown, K. O. Mikaelian, R. J. Gould, et al., *Absorption of High-Energy Cosmic Photons through Double-Pair Production in Photon-Photon Collisions Astrophys. Lett.*, **14** (1973), pp. 203-205

[10] R. T. Coogan, A. M. Brown, and P. M. Chadwick, *Localising the γ-ray emission region during the June 2014 outburst of 3C 454.3*, Accepted for publication in *MNRAS*, arXiv:1601.07180v1 [astro-ph.HE] (2016), 12 pages

[11] A. Dotson, M. Georganopoulos, D. Kazanas, and E. S. Perlman, *A Method for Localizing Energy Dissipation in Blazars Using Fermi Variability*, *ApJL*, **758** (2012), pp. L15-L19

[12] J. D. Finke, C. D. Dermer and M. Böttcher, *Synchrotron Self-Compton Analysis of TeV X-Ray-Selected BL Lacertae Objects*, *ApJ*, **686** (2008), pp. 181-194

[13] J. D. Finke, *Modeling Fermi Large Area Telescope and Multiwavelength Data from Blazars*, *Proceedings of Science*, PoS(HEASA2015)006 (2015), 21 pages, *(in these proceedings)*

[14] R. J. Gould, and G. P. Schréder, *Opacity of the Universe to High-Energy Photons Phys. Rev.*, **155** (1967), pp. 1408-1411

[15] S. G. Jorstad, A. P. Marscher, M. L. Lister, et al., *Polarimetric Observations of 15 Active Galactic Nuclei at High Frequencies: Jet Kinematics from Bimonthly Monitoring with the Very Long Baseline Array*, *AJ*, **130** (2005), pp. 1418-1465

[16] K. Nalewajko, M. C. Begelman, and M. Sikora, *Constraining the Location of Gamma-Ray Flares in Luminous Blazars*, *ApJ*, **789** (2014), pp. 161-180

[17] M. Orienti, S. Koyama, F. D'Ammando, et al., *Radio and γ-ray follow-up of the exceptionally high-activity state of PKS 1510-089 in 2011*, *MNRAS*, **428** (2013), pp. 2418-2429

[18] The Planck Collaboration: P. A. R. Ade, N. Aghanim, C. Armitage-Caplan, et al., *Planck 2013 results. XVI. Cosmological parameters*, *A&A*, **571** (2014), A16, 66 pages

[19] M. Sikora, R. Moderski, and G. M. Madejski, *3C 454.3 Reveals the Structure and Physics of Its "Blazar Zone"*, *ApJ*, **675** (2008), pp. 71-78

[20] T. Sbarrato, G. Ghisellini, L. Maraschi and M. Colpi, *The relation between broad lines and γ-ray luminosities in Fermi blazars*, *MNRAS*, **421** (2012), pp. 1764-1778

[21] Y. Tachibana, N. Kawai and S. Pike, et al., *A Correlation Between Optical, X-ray, and Gamma-ray Variations in Blazar 3C 454.3*, in proceedings of the *Fifth Fermi Symposium*, arXiv:1502.03610 [astro-ph.HE] (2015), 6 pages

[22] C. M. Urry & P. Padovani, *Unified Schemes for Radio-Loud Active Galactic Nuclei*, *PASP*, **107** (1995), pp. 803-845

[23] S. Vercellone, A. W. Chen, V. Vittorini, et al., *Multiwavelength Observations of 3C 454.3. I. The AGILE 2007 November campaign on the "Crazy Diamond"*, *ApJ*, **690** (2009), pp. 1018-1030

[24] S. Vercellone, F. D'Ammando, V. Vittorini, et al., *Multiwavelength Observations of 3C 454.3. III. Eighteen Months of Agile Monitoring of the "Crazy Diamond"*, *ApJ*, **712** (2010), pp. 405-420